The current issue and full text archive of this journal is available at
www.emeraldinsight.com/0332-1649.htm

Eddy current brake with two pole pairs

Eckhard Baum
University of Applied Sciences Fulda, Fulda, Germany, and
Stefan Eberhardt
Josef Wiegand GmbH & Co. KG Freizeiteinrichtungen, Germany

Abstract

Purpose – The purpose of this paper is to derive a force-velocity characteristic for an eddy current brake with minor computational effort.

Design/methodology/approach – The speed range is split into two domains. While in the low-speed domain it is possible to achieve a closed form expression for the force-velocity characteristic in the high-speed region approximations have to be introduced.

Findings – The derived relation for the force-velocity characteristic has been compared with measurement results. The comparison shows that the approach yields good results for not too large air gaps.

Originality/value – A combination of analytical and approximative methods has been used for the determination of the force-velocity characteristic of an eddy current brake with two pole pairs.

Keywords Eddy currents, Velocity, Electromagnetism, Numerical analysis

Paper type Research paper

1. Introduction

In this paper, an eddy current brake according to Figure 1(a) is considered. A permanent magnet arrangement at a radial distance c is placed over a conducting thin disk of radius A. The permanent magnet arrangement consists of two pole pairs, see Figure 1(b), each pole having a volume $a_M \times b_M \times h_M$.

It is shown in detail in Figure 1(b). In the middle of the air gap of length $2d_{\mathrm{Air}} + 2d_{\mathrm{CuH}}$ the conducting disk of thickness $2d_{\mathrm{CuH}}$ is rotating with angular velocity ω. The coordinate system used (not shown in the figures) is cylindrical with its z-axis coinciding with the axis of rotation. The purpose of the analysis is to obtain the force-velocity characteristic of the brake.

This is achieved in treating the low- and the high-velocity region separately. In the low-velocity region first a disk with infinite radius is considered. The current distribution in a disk with finite radius is then constructed using mirror magnets over the infinite disk. The current distribution due to two pole pairs is ascribed to the superposition of the current distributions due to one pole pair. Even in the high-velocity region the relation:

$$\frac{1}{\sqrt{\frac{1}{2}\,\omega\kappa\mu_{\mathrm{D}}}} \gg 2d_{\mathrm{CuH}}, \tag{1}$$

The authors thank Josef Wiegand GmbH & Co. KG, Germany for the generous support of this work.

COMPEL: The International Journal for Computation and Mathematics in Electrical and Electronic Engineering
Vol. 28 No. 1, 2009
pp. 67-76

0332-1649
DOI 10.1108/03321640910918878

where κ and μ_D are the disk conductivity and permeability, is assumed to hold leading to an $z-$independent current distribution in the disk. It is further assumed that the current density $\vec{J}$ has only in plane components for displacement currents are neglected even in the high-speed domain. Therefore, the area resistivity:

$$\bar{\rho} = \frac{\rho}{2d_{\mathrm{CuH}}}, \tag{2}$$

and the surface current:

$$\vec{i} = \vec{J} \cdot 2d_{\mathrm{CuH}}, \tag{3}$$

are introduced.

The permanent magnets are assumed to have rigid magnetization M. For the analytical treatment the rectangular pole face $a_M \times b_M$ is replaced by a circular face with radius a.

2. Low-rotational frequencies

Equation (1) holds in the low and in the high-frequency regime. In the low-frequency regime, it is further assumed that:

$$\frac{\bar{\rho}}{\mu_D} \gg \omega c. \tag{4}$$

2.1 Disk with infinite radius

Smythe (1989, 1942) referring to Maxwell gives a formula for the vector potential solely due to the eddy currents in the disk in presence of field exciting sources (index: exc) above the disk in $z > 0$. It also holds in similar form for the scalar potential V reading:

$$V(x,y,z,t) = \mathrm{sign}(z) \int_0^\infty \frac{\partial}{\partial t} V_{\mathrm{exc}}\left(x, y, -|z| - \frac{2\bar{\rho}}{\mu_D}\tau, t - \tau\right) \mathrm{d}\tau. \tag{5}$$

The exciting scalar potential is that of magnetic charges in $z = h : d_{\mathrm{Air}} + d_{\mathrm{CuH}}$ representing one pole of radius a above the disk. At $t = 0$, $\varphi = \phi$, see Figure 2:

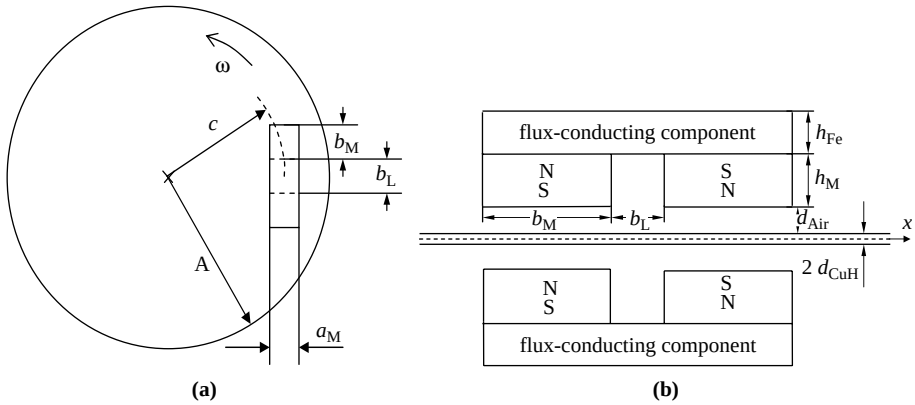

Figure 1.
(a) Permanent magnets over rotating conducting disk; (b) permanent magnet arrangement consisting of two pole pairs

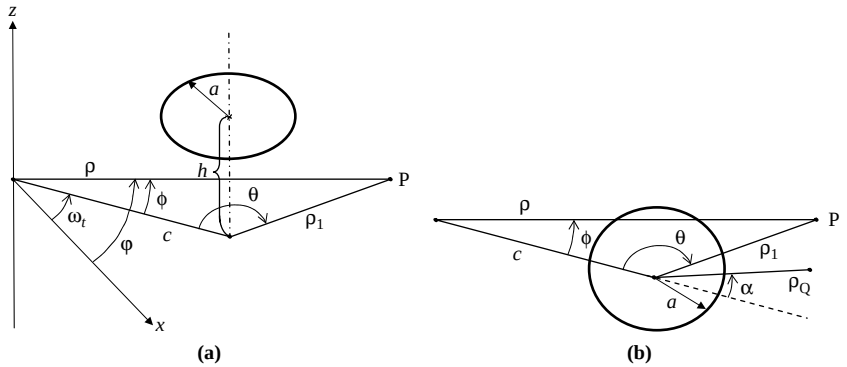

Notes: (a) Pole of radius a rotating above disk with infinite radius covering the plane $z = 0$. Point P with cylindrical coordinates ρ and φ is fixed in $z = 0$. Coordinates ϕ and θ change while the pole rotates; (b) same as 2a,but top view

Figure 2.

$$V_{\text{exc}}(\rho, \varphi, z = 0, t = 0) = \frac{1}{4\pi}\int_0^a \int_0^{2\pi} \frac{M\rho_Q \mathrm{d}\rho_Q \mathrm{d}\alpha}{\sqrt{h^2 + \rho_Q^2 + \rho_1^2 - 2\rho_1\rho_Q \cos[\pi - \theta - \alpha]}} = \frac{1}{4\pi}\int_0^a \int_0^{2\pi} \frac{M\rho_Q \mathrm{d}\rho_Q \mathrm{d}\alpha}{\sqrt{h^2 + \rho_Q^2 + \rho_1^2 - 2\rho_1\rho_Q \cos\alpha}}, \tag{6}$$

with:

$$\rho_1 = \sqrt{c^2 + \rho^2 - 2\rho c \cos\varphi}, \tag{7}$$

which follows from the law of cosine in Figure 2(a).

For $t > 0$ the distance ρ_1 must be replaced by:

$$\rho_1(t) = \sqrt{c^2 + \rho^2 - 2\rho c \cos(\varphi + \omega t)}, \tag{8}$$

left-handed rotation presumed.

Application of equation (5) yields:

$$V(\rho, \varphi, z = 0, t) = \frac{1}{4\pi} \cdot \int_0^a \int_0^{2\pi} \int_0^{\infty} \frac{\partial}{\partial t} \frac{M\rho_Q \mathrm{d}\rho_Q \mathrm{d}\alpha \mathrm{d}\tau}{[(h + (2\bar{\rho}\tau/\mu_D))^2 + \rho_Q^2 + \rho_1^2(t,\tau) - 2\rho_1(t,\tau)\rho_Q \cos\alpha]}, \tag{9}$$

with:

$$\rho_1(t, \tau) = \sqrt{c^2 + \rho^2 - 2\rho c \cos(\varphi + \omega(t - \tau))}. \tag{10}$$

But in equation (9) the term with τ^2 quickly dominates the denominator with increasing τ, so $\rho_1(t,\tau)$ can be substituted by $\rho_1(t)$. Finally, for $t = 0$:

$$V(\rho, \varphi, z = 0, t = 0) = -\frac{1}{4\pi} \cdot \int_0^a \int_0^{2\pi} \int_0^{\infty} \frac{\rho_1 - \rho_Q \cos\alpha}{[(h + (2\bar{\rho}\tau/\mu_D))^2 + \rho_Q^2 + \rho_1^2 - 2\rho_1\rho_Q\cos\alpha]^{3/2}} \cdot \frac{\omega\rho c \sin(\varphi)}{\rho_1} M \rho_Q \mathrm{d}\rho_Q \mathrm{d}\alpha \mathrm{d}\tau \tag{11}$$

For $h \ll a, h$ can be neglected in equation (11). Further calculations then yield:

$$\begin{aligned} V(\rho, \varphi, z = 0, t = 0) &= -\frac{M\omega\rho c \sin\varphi}{\rho_1} \frac{\mu_D}{2\bar{\rho}} \\ &\quad \times \frac{1}{4\pi} \int_0^a \int_0^{2\pi} \int_0^{\infty} \frac{\rho_1 - \rho_Q \cos\alpha}{[u^2 + \rho_Q^2 + \rho_1^2 - 2\rho_1\rho_Q\cos\alpha]^{3/2}} \rho_Q \mathrm{d}\rho_Q \mathrm{d}\alpha \mathrm{d}u \\ &= -\frac{M\omega\rho c \sin\varphi}{\rho_1} \frac{\mu_D}{2\bar{\rho}} \frac{1}{4\pi} \int_0^a \int_0^{2\pi} \frac{\rho_1 - \rho_Q \cos\alpha}{\rho_Q^2 + \rho_1^2 - 2\rho_1\rho_Q\cos\alpha} \rho_Q \mathrm{d}\rho_Q \mathrm{d}\alpha \end{aligned} \tag{12}$$

The current function $\Phi(P)$ giving the current between point P and infinity is related to the scalar potential V by:

$$\Phi(\rho_0, \varphi_0, t) = 2V(\rho_0, \varphi_0, z = +0, t), \tag{13}$$

see (Smythe, 1989).

Using:

$$\int_0^{2\pi} \frac{\rho_1 - \rho_Q \cos\alpha}{\rho_Q^2 + \rho_1^2 - 2\rho_1\rho_Q\cos\alpha} \mathrm{d}\alpha = \begin{cases} 2\pi/\rho_1 & \text{for } \rho_Q < \rho_1 \\ 0 & \text{for } \rho_Q > \rho_1 \end{cases},$$

one gets for equation (12):

$$V(\rho, \varphi, z = 0, t = 0) = -\frac{M\omega\rho c \sin\varphi}{4\pi\rho_1} \frac{\mu_D}{2\bar{\rho}} \begin{cases} \frac{\pi}{\rho_1} a^2 & f\ddot{u}r \ a < \rho_1 \\ \frac{\pi}{\rho_1} \rho_1^2 & f\ddot{u}r \ a > \rho_1 \end{cases} \tag{14}$$

From the last formula the current function excited by two poles, one above and one below the disk, can be derived to be:

$$\Phi(\rho, \varphi, t = 0) = -\frac{M\omega\rho c \sin\varphi}{\rho_1^2} \frac{\mu_D}{2\bar{\rho}} \begin{cases} a^2 & \text{for } a < \rho_1 \\ \rho_1^2 & \text{for } a > \rho_1 \end{cases}, \tag{15}$$

see (Smythe, 1989).

2.2 Disk with finite radius

The eddy current distribution in a disk with finite radius A is obtained by retaining the infinite disk and the first pole pair (Figure 3) and introducing a second pole pair with:

$$a' = \frac{A}{c}\,a,\quad c' = \frac{A^2}{c},\quad h' = \frac{A}{c}\,h,\quad M' = -\frac{c^2}{A^2}\,M. \tag{16}$$

It can be shown that under condition (4) the current functions of the two pole pairs cancel on $\rho = A$. In Smythe (1989), the current function for the original pole pair plus the mirror pole pair is shown to be:

$$\Phi(\rho, \varphi, t=0) = M\omega\rho\sin\varphi a^2\frac{\mu_D}{2\bar{\rho}}\begin{cases}\frac{c}{c^2+\rho^2-2\rho c\cos\varphi} - \frac{A^2/c}{\rho^2+(A^4/c^2)-2\rho(A^2/c)\cos\varphi}\\ \frac{c}{a^2} - \frac{A^2/c}{\rho^2+(A^4/c^2)-2\rho(A^2/c)\cos\varphi}\end{cases}, \tag{17}$$

the upper line being valid for $\rho_1 > a$, the lower line for $\rho_1 < a$.

2.3 Torque on one pole pair

The torque on the currents under the original pole is obtained by:

$$\begin{aligned} T_z &= \mu_0 M\iint_F \rho\cdot\frac{\partial\Phi}{\rho\partial\varphi}\cdot\mathrm{d}F = \frac{M^2\mu_0\mu_D\omega a^2}{2\bar{\rho}} \\ &\cdot\iint_F\left[\frac{\partial}{\partial\varphi}\,\frac{c\rho\sin\varphi}{a^2} - \frac{\partial}{\partial\varphi}\,\frac{c'\rho\sin\varphi}{\rho^2+c'^2-2\rho c'\cos\varphi}\right]\mathrm{d}F. \end{aligned} \tag{18}$$

After some manipulations a closed form integration is possible yielding:

$$T_z = \frac{M^2\mu_0\mu_\mathrm{D}\omega c^2\cdot\pi a^2}{\bar{\rho}}\cdot c_\mathrm{Korr}(A,c) = \frac{M^2\mu_0\mu_\mathrm{D}\omega c^2\cdot\pi a^2}{\bar{\rho}}\cdot\frac{1}{2}\left(1-\frac{A^2a^2}{(A^2-c^2)^2}\right). \tag{19}$$

Note that in equation (19) the factor c_Korr is introduced (Wouterse, 1991) accounting for the non perfect conductivity outside the area $F = \pi a^2$ shadowed by the original pole pair.

2.4 Torque on two pole pairs

If a second pole pair at $\rho = c$, $\phi = \phi_0$ is present, the current function shadowed by the first pole pair must be corrected by:

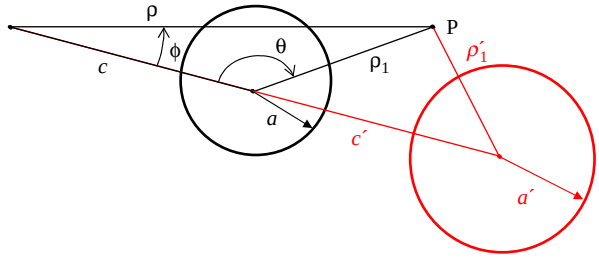

Figure 3.
Original and mirror pole

$$\Phi_2(\rho,\varphi,t=0) = -M\omega\rho\sin(\varphi-\varphi_0)a^2\frac{\mu_D}{2\bar{\rho}} \cdot \begin{cases} \left[\frac{c}{c^2+\rho^2-2\rho c\cos(\varphi-\varphi_0)} - \frac{A^2/c}{\rho^2+(A^4/c^2)-2\rho(A^2/c)\cos(\varphi-\varphi_0)}\right] \\ \left[\frac{c}{a^2} - \frac{A^2/c}{\rho^2+(A^4/c^2)-2\rho(A^2/c)\cos(\varphi-\varphi_0)}\right] \end{cases}, \tag{20}$$

the upper lines holding outside the area shadowed by the second pole pair, the lower lines holding inside.

This leads to an additional moment:

$$\begin{aligned} \Delta T_z &= -\mu_0 M \iint_F \rho \cdot \frac{\partial \Phi_2}{\rho \partial \varphi} \cdot \mathrm{d}F \\ &= \mu_0 M \iint_F \frac{\partial \Phi_2}{\partial \varphi}\mathrm{d}F \\ &= \frac{M^2\mu_0\mu_D\omega a^2\pi c^2}{2\bar{\rho}} \cdot \left(\frac{1}{\pi c^2}\iint_F - \frac{\partial}{\partial\varphi}\,\frac{c\rho\sin(\varphi-\varphi_0)}{c^2+\rho^2-2\rho c\cos(\varphi-\varphi_0)}\mathrm{d}F \right. \\ &\quad \left. + \underbrace{\frac{1}{\pi c^2}\iint_F \frac{\partial}{\partial\varphi}\,\frac{c'\rho\sin(\varphi-\varphi_0)}{\rho^2+c'^2-2\rho c'\cos(\varphi-\varphi_0)}\mathrm{d}F}_{t_z} \right) \end{aligned} \tag{21}$$

Hence, on an arrangement with two pole pairs according to Figure 1, the force retarding the disk is:

$$F_0 = 2\cdot\kappa v B_0^2 \cdot a_M b_M 2d_{\mathrm{CuH}} \cdot c'_{\mathrm{Korr}}, \tag{22}$$

proportional to the velocity v, where:

$$c'_{\mathrm{Korr}} = c_{\mathrm{Korr}} + \Delta t_z. \tag{23}$$

Figure 4 shows the magnetic field for small rotational speed obtained by a 2D finite element analysis (FEA). FEA is used to determine the effective pole face and air gap induction.

3. High rotational frequencies-exact solution

3.1 Disk with infinite radius

In a first step the scalar potential of magnetic charges above the disk in $z = h$: $d_{\mathrm{Air}} + d_{\mathrm{CuH}}$ representing one pole of radius a is written down:

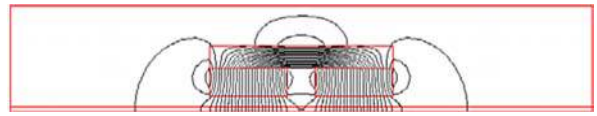

Note: 2D FEM analysis for low-rotational speed

Figure 4.
Magnetic field in arrangement with two pole pairs

$$V_{\mathrm{exc}}(\rho_1, z) = \frac{aM}{2} \int_0^\infty \frac{1}{k} J_0(k\rho_1) J_1(ka) \mathrm{e}^{-k(h-z)} \mathrm{d}k, \tag{24}$$

using a cylindrical coordinate system with its axis coinciding with the axis of the circular area, see Figure 2.

Using equation (5) one gets for the eddy current scalar potential on:

$$\rho = A \Leftrightarrow \rho_1 = \sqrt{c^2 + A^2 - 2cA\cos\phi}, \tag{25}$$

$$\begin{aligned} &V(\rho = A, \varphi, z, t) \\ &\quad = \frac{1}{2} aM \cdot \int_0^\infty \frac{\partial}{\partial t} \int_0^\infty \frac{1}{k} \mathrm{J}_0\left(k\sqrt{c^2 + A^2 - 2cA\cos[\varphi - \omega(t-\tau)]}\right) \\ &\qquad \cdot \mathrm{J}_1(ka) e^{-k(h+|z|+(2\bar{\rho}/\mu_{\mathrm{F}})\tau)} \mathrm{d}k\mathrm{d}\tau. \end{aligned} \tag{26}$$

3.2 Disk with finite radius

As in the low frequency case of Section 2. B a mirror pole is introduced in $c' = A^2/c$ with altered radius a' and height h'. The scalar potential of the eddy currents related to this mirror pole on:

$$\rho = A \Leftrightarrow \rho_1' = \sqrt{c'^2 + A^2 - 2c'A\cos\phi}, \tag{27}$$

is:

$$\begin{aligned} &V'(\rho = A, \varphi, z, t) \\ &\quad = \int_0^\infty \frac{\partial}{\partial t} V'_{\mathrm{exc}}\left(\rho, \varphi, -|z| - \frac{2\bar{\rho}}{\mu_D}\tau, t - \tau\right) \mathrm{d}\tau \\ &\quad = \frac{1}{2} a'M' \int_0^\infty \frac{\partial}{\partial t} \int_0^\infty \frac{1}{k} J_0\left(k\sqrt{c'^2 + A^2 - 2c'A\cos[\varphi - \omega(t-\tau)]}\right) \\ &\qquad \cdot J_1(ka') \mathrm{e}^{-k(h'+|z|+(2\bar{\rho}/\mu_{\mathrm{D}})\tau)} \mathrm{d}k\mathrm{d}\tau \\ &\quad = \frac{1}{2} a'M' \int_0^\infty \frac{\partial}{\partial t} \int_0^\infty \frac{1}{k} J_0\left(k\frac{A}{c}\sqrt{c^2 + A^2 - 2cA\cos[\varphi - \omega(t-\tau)]}\right) \\ &\qquad \cdot J_1(k(A/c)a) \mathrm{e}^{-k((A/c)h+|z|+(2\bar{\rho}/\mu_{\mathrm{D}})\tau)} \mathrm{d}k\mathrm{d}\tau \\ &\quad = \frac{1}{2} a'M' \int_0^\infty \frac{\partial}{\partial t} \int_0^\infty \frac{1}{\bar{k}} J_0\left(\bar{k}\sqrt{c^2 + A^2 - 2cA\cos[\varphi - \omega(t-\tau)]}\right) \\ &\qquad \cdot J_1(\bar{k}a) \mathrm{e}^{-\bar{k}(h+(c/A)|z|+(c/A)(2\bar{\rho}/\mu_{\mathrm{D}})\tau)} \mathrm{d}\bar{k}\mathrm{d}\tau. \end{aligned} \tag{28}$$

The above mirror potential cancels the potential of the original pole on $\rho = A$ if, in contrast to equation (16):

$$a' = \frac{A}{c} a, \quad c' = \frac{A^2}{c}, \quad h' = \frac{A}{c} h, \quad M' = -\frac{c}{A} M, \tag{29}$$

and the area resistance is changed into:

$$\bar{\rho}' = \frac{A}{c}\bar{\rho}. \tag{30}$$

However, the last relation is unacceptable. Hence, the high-frequency regime is treated in a different way.

4. High rotational frequencies-approximate solution

In this section, the disk with finite radius is treated without pertaining to the infinite disk. Following Wouterse (1991), it is assumed that for high-rotational speed the consumed power tends to a limiting value, hence the flux crossing the disk must tend to zero. A sketch of the supposed field distribution for high-rotational speed is shown in Figure 5.

The normal air gap induction becomes approximately zero if in two closed channels surrounding the areas shadowed by the poles the current:

$$I_\infty = h_M \frac{B_r}{\mu_0}, \tag{31}$$

flows. Each of the channels has its maximum resistance:

$$R_1 = \frac{1}{\kappa}\,\frac{a_M}{2d_{\mathrm{CuH}}\cdot(b_L/2)}, \tag{32}$$

on the way between the pole areas, the resistance of the other channel segments is neglected. This in itself is rather simplifying; furthermore the formation of multiple eddy current paths has to be expected for large air gaps which is also not covered by the above supposition.

Equating the electric power in the disk with the mechanical power $F_\infty\, v$ one gets:

$$F_\infty = 2\cdot\frac{1}{v}I_\infty^2 R_1 = 2\cdot\frac{1}{v}\left(h_M\frac{B_r}{\mu_0}\right)^2\frac{1}{\kappa}\,\frac{a_M}{2d_{\mathrm{CuH}}\cdot(b_L/2)} = 2\cdot\frac{1}{v}h_M^2\frac{B_r^2}{\mu_0^2}\,\frac{1}{\kappa}\,\frac{a_M}{d_{\mathrm{CuH}}b_L}. \tag{33}$$

The factor 2 accounts for the two current channels.

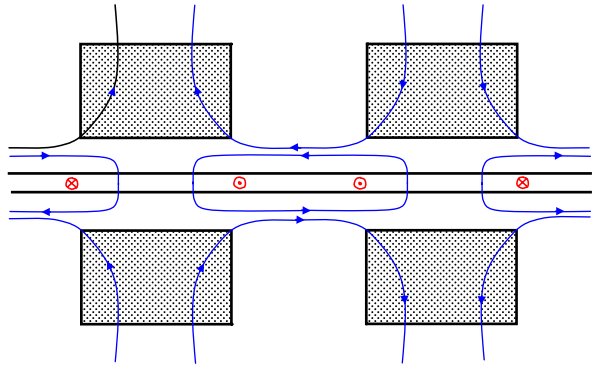

Figure 5.
Supposed magnetic field in arrangement with two pole pairs for high rotational speed

5. Combining the low and high speed domains

The critical velocity is defined by postulating that the forces in (22) and (33) shall be equal at this velocity, hence:

$$v_{\text{krit}} = \frac{h_M}{\sqrt{2}d_{\text{CuH}}} \frac{B_r}{\mu_0 B_0} \frac{1}{\kappa} \sqrt{\frac{1}{b_L b_M} \frac{1}{c'_{\text{Korr}}}}. \tag{34}$$

At this velocity the maximum force is expected to be exerted on the disk leading to the ansatz (Wouterse, 1991):

$$F(v) = F_{\text{krit}} \frac{2}{(v/v_{\text{krit}}) + (v_{\text{krit}}/v)}. \tag{35}$$

For low velocities equation (35) must coincide with equation (22) yielding:

$$F_{\text{krit}} = 2 \cdot a_M \cdot \frac{h_M}{\sqrt{2}} \frac{B_0 B_r}{\mu_0} \sqrt{\frac{b_M}{b_L} c'_{\text{Korr}}}, \tag{36}$$

for the critical force.

6. Example

For $d_{\text{CuH}} = 3\,\text{mm}$, $d_{\text{Air}} = 9.5\,\text{mm}$, $b_{\text{M}} = 70\,\text{mm}$, $b_{\text{L}} = 25\,\text{mm}$, $h_{\text{Fe}} = 20\,\text{mm}$ (Figure 1) the measured and the computed force-velocity characteristic have been shown in Figure 6. The disk was made of copper (water-cooled while moving), for the permanent magnets NdFeB was employed. The effective air gap induction was determined with the help of a 2D FEA noting that the magnetic resistance of the air gap needs to be adjusted. Unfortunately, especially for large air gaps, the deviation between measurement and computation may become unacceptably high.

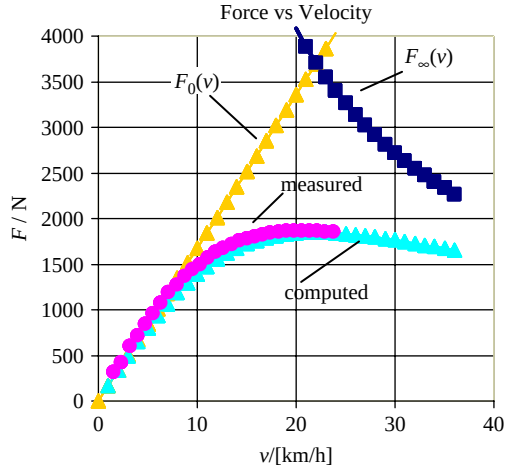

Figure 6.
Comparison of measured and computed force-velocity characteristic

7. Conclusions

The force-velocity-relation for an eddy current brake with two pole pairs has been computed by splitting the speed range into two domains. In the low-speed domain closed form expressions can be derived. However, mirroring of field exciting sources as in the low-speed domain becomes problematical for high speeds. Therefore, an approximate method is introduced based on the assumption that in the high-speed domain the power consumed by the disk is independent of velocity.

References

Smythe, W.R. (1942), "On eddy currents in a rotating disk", *Transactions AIEE*, Vol. 61, pp. 681-4.

Smythe, W.R. (1989), *Static and Dynamic Electricity*, 3rd ed., Hemisphere Publishing Corporation, New York, NY.

Wouterse, J.H. (1991), "Critical torque and speed of eddy current brake with widely separated soft iron poles", *IEE Proceedings-B*, Vol. 138 No. 4, pp. 153-8.

Further reading

Abramov, A.D. (1971), "Eddy-current loss in a rotating magnetic field", *Russian Physics Journal*, Vol. 14 No. 1, pp. 25-8.

Hartz, G. (1985), "Numerische Berechnung der Felder, Wirbelströme und Kräfte in einer linearen Wirbelstrombremse mit magnetischer Reaktionsschiene", dissertation, RWTH Aachen, Aachen.

Lee, K. and Park, K. (2002), "Analysis of an eddy-current brake considering finite radius and induced magnetic flux", *Journal of Applied Physics*, Vol. 92 No. 9, pp. 5532-8.

Nehl, T.W. and Lequesne, B. (1994), "Nonlinear two-dimensional finite element modelling of permanent magnet eddy current couplings and breaks", *IEEE Trans.on Magnetics*, Vol. 30 No. 5, pp. 3000-3.

Philippow, E. (1976), *Taschenbuch der Elektrotechnik*, Band 1.VEB Verlag Technik, Berlin.

Schieber, D. (1972), "Unipolar induction braking of thin metal sheets", *Proc. IEE*, Vol. 119 No. 10, pp. 1499-503.

Schieber, D. (1974), "Braking torque on rotating sheet in stationary magnetic field", *Proc. IEE*, Vol. 121 No. 2, pp. 117-22.

About the authors

Eckhard Baum holds a PhD in Engineering and is Professor for Fundamentals of Electrical Engineering. He works at the University of Applied Sciences in Fulda, Germany. His research interests cover the topics electromagnetic field theory, electromagnetic compatibility, analytical and numerical computation of electromagnetic fields.

Stefan Eberhardt is with Josef Wiegand GmbH & Co. KG Freizeiteinrichtungen, Germany. His area of responsibility is related to the design of summer toboggan runs.